Modelling and design of grid voltage oriented vector control scheme for DC railway recuperating system

Chuen Ling Toh[1], Chee Wei Tan[2]
[1]Institute of Power Engineering, Universiti Tenaga Nasional, Kajang, Malaysia
[2]Department of Electrical Power Engineering, Faculty of Electrical Engineering, Universiti Teknologi Malaysia, Skudai, Malaysia

Article Info

ABSTRACT

The braking energy harvested by a railway vehicle can be restored to the utility grid with a power recuperating system. A grid connected voltage source inverter (VSI) is commonly used as a grid-feeding converter in the recuperating system. This paper proposes to integrate grid voltage oriented vector control (GVOVC) and third harmonic voltage injection pulse width modulation (THVI-PWM) technique for the VSI to ensure grid voltage and frequency synchronization. A simulation study is carried out to evaluate the feasibility of the proposed control and modulation schemes using MATLAB/Simulink. The results show that the proposed controller may reach steady-state operating mode within 7 ms by producing good quality AC voltages and currents waveforms. With the independent control of voltage quantities in dq reference frame, the regulation of active and reactive power could be realized.

Corresponding Author:

Chuen Ling Toh
Institute of Power Engineering, Universiti Tenaga Nasional
Kajang, Malaysia
Email: chuenling@uniten.edu.my

1. INTRODUCTION

A traditional DC railway power substation used to employ twelve-pulse rectifier transformer system as shown in Figure 1 [1]–[3]. This configuration aims to minimize the DC voltage ripples and eliminate the low order AC current harmonics [4]. However, as the traction rectifier is uncontrolled, power resistors must be activated to comsume braking energies harvested by a stopping train Figure 1(a). Literatures [5], [6], had proposed to introduce a DC power recuperating system to transmit the braking energy back to the utility grid. Some simulation studies have concluded that about 10% to 40% of energy saving could be achieved with a recuperating system [7], [8]. The recuperating system is connected in parallel with the existing twelve-pulse rectifier transformer system as shown in Figure 1(b). Three typical components namely voltage source inverter (VSI), passive filters, and recovery transformer must be employed. The regenerative DC power will first be inverted using a pulse-width-modulated VSI [9], [10]. The generated AC voltages may contain high frequency switching harmonics, thus, passive filters are demanded to purify the waveshapes [11], [12]. The recovery transformer is used to step up the AC voltage level to meet with the utility grid power ratings [13].

The VSI used in this application can be classified as a grid-feeding power converter [14], which mainly used to deliver regenerative power to an energized grid. Some established linear control schemes had been proposed for grid-feeding converters, which include proportional-integral (PI) [15], and adaptive controllers [16]. These controllers had been studied, compared and evaluated for distributed power generation [17], [18], AC microgrid [19] and traction power supply [20]. Since, the synchronization of the AC voltages at the point of coupling is the key to enabling power exchanged accurately, this paper proposes to integrate grid

voltage oriented vector control (GVOVC) for the VSI in a traction power substation. As the grid voltages are sampled and feedforward in the controller, a small variation in grid voltage will be corrected immediately using a simple PI-controller. In addition, to enhance the utilization of the DC-link voltage of the VSI, the third harmonic voltage injection pulse width modulation (THVI-PWM) technique will be applied [21]–[23]. In short, this paper will present the mathematical modelling of the GVOVC in section 2. Section 3 presents the PI-controller gain tunning and analysis. A system level simulation study of a DC power recuperating system with the proposed controller is presented in section 4. Lastly, section 5 concludes the research findings of this simulation study.
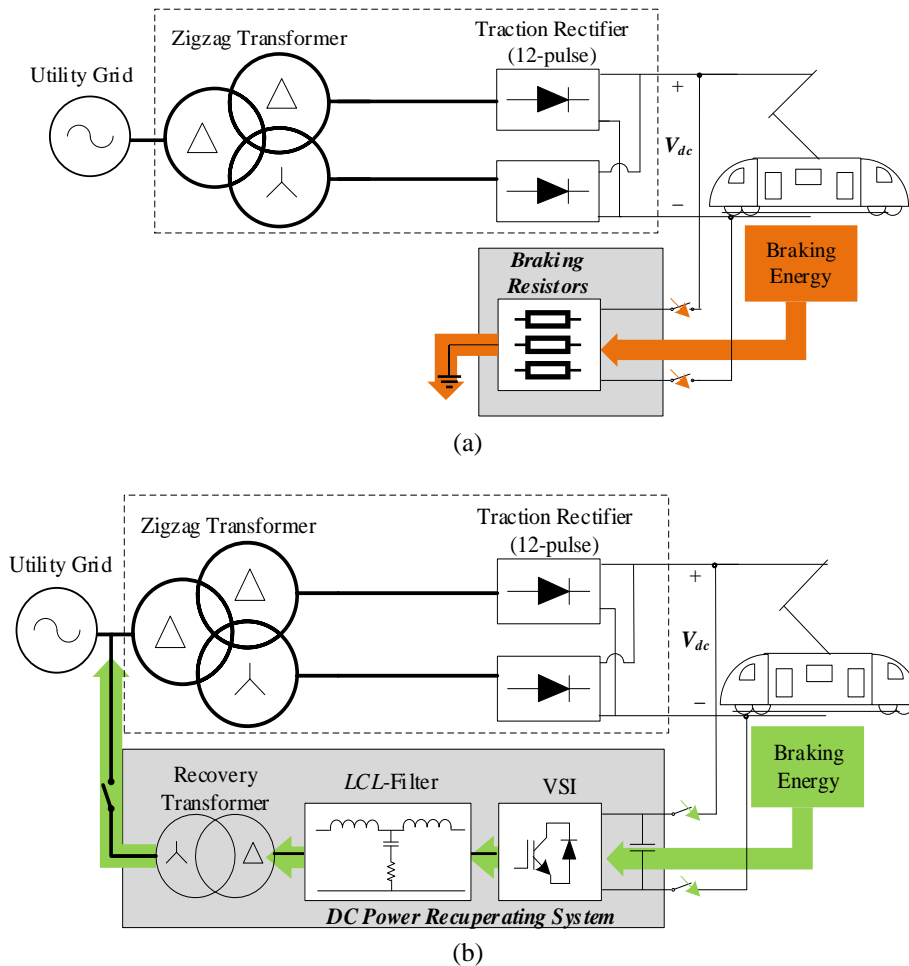

(a)

(b)

Figure 1. Braking energy management at DC power substation (a) DC power dissipation via braking resistor banks and (b) DC power regeneration inverter system

2.   MODELLING OF RECUPERATING SYSTEM

An equivalent circuit of recuperating system is shown in Figure 2. When a train starts to break, it will act as an electrical generator. This may increase the DC-link voltage, V_{dc}, to it maximum level. Assume that the DC-link voltage is under controlled, the braking current, i_{br}, will flow into the DC terminal of the VSI. The VSI is used to process and deliver the braking energy back to the utility grid. As the VSI operates in high switching frequency, a three-phase LCL filter will be employed to mitigate the switching noises. The recovery transformer and utility grid shown in Figure 1(b) are modelled as wye-connected AC supplies, v_{xg}, with internal resistance, R_g, and reactance, L_g.

The following sub-section will present the mathematical modelling of LCL filter and GVOVC. It is highlighted that the mathematical modelling of DC link and VSI [15], the LCL filter design methodology [11], [12] and the THVI-PWM techniques [22], [23] will not be presented in this paper. All technical details can be referred from the above-mentioned literatures.
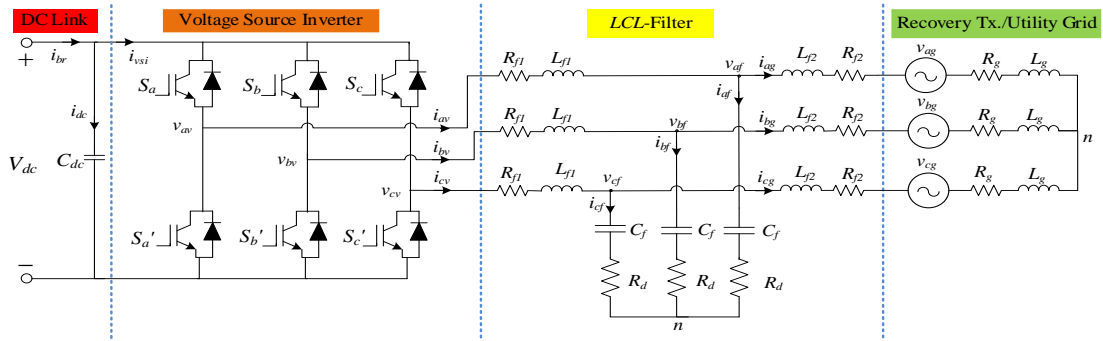
Figure 2. Equivalent circuit of recuperating system

2.1. Recuperating system modeling with LCL filter

As shown in Figure 2, the LCL filter is connected in wye configuration. Each phase of the LCL-filter consists of converter-side inductance, L_{f1}, with its internal resistance, R_{f1}, grid-side inductance, L_{f2}, with its internal resistance, R_{f2}, filter capacitance, C_f, and a damping resistor, R_d. Since the LCL-filter is designed with identical parameters for all the phases, the voltage drop across the filtering capacitors and damping resistor, v_{xf}, can be simplified as:

$$v_{xf} = R_d i_{xf} + \frac{1}{C_f} \int i_{xf}\, dt \tag{1}$$

the subscription x represents phases of a, b, and c. In addition, the currents being drain out by the filter capacitor can be derived using the classic Kichoff Current Law.

$$i_{xf} = i_{xv} - i_{xg} \tag{2}$$

Theoretically, i_{xf} should contains all the switching harmonics produced by the VSI, so that sinusoidal grid currents, i_{xg}, and voltages, v_{xg}, will be produced at the point of coupling. Consequently, a set of converter's voltage equations can be further elaborated by taking into account all the filters parameters.

$$v_{xv} = R_{f1} i_{xv} + L_{f1} \frac{di_{xv}}{dt} + R_{f2} i_{xg} + L_{f2} \frac{di_{xg}}{dt} + v_{xg} + R_g i_{xg} + L_g \frac{di_{xg}}{dt} \tag{3}$$

2.2. GVOVC

The control scheme proposes in this paper used to align the AC voltages with the orientation of grid voltage space-vector [24]. This control strategy can be easily being developed using the dq-components of a system model. Thus, a set of dynamic model equations must first be outlined. Referring to (3), the recovery transformer and utility grid are assumed ideal (by neglecting R_g, and L_g), the three-phase voltage equations can then be transformed to $\alpha\beta$ reference frame using two mathematical expressions as:

$$v_{\alpha v} = R_{f1} i_{\alpha v} + L_{f1} \frac{di_{\alpha v}}{dt} + R_{f2} i_{\alpha g} + L_{f2} \frac{di_{\alpha g}}{dt} + v_{\alpha g} \tag{4}$$

$$v_{\beta v} = R_{f1} i_{\beta v} + L_{f1} \frac{di_{\beta v}}{dt} + R_{f2} i_{\beta g} + L_{f2} \frac{di_{\beta g}}{dt} + v_{\beta g} \tag{5}$$

In (4) and (5) can be presented using space vector notation:

$$\vec{v}_v^s = R_{f1} \vec{i}_v^s + L_{f1} \frac{d\vec{i}_v^s}{dt} + R_{f2} \vec{i}_g^s + L_{f2} \frac{d\vec{i}_g^s}{dt} + \vec{v}_g^s \tag{6}$$

where the superscript s of (6) means for electrical quantities referring to stationary reference frame. In order to transform all the stationary quantities into synchronous rotatory reference frame, (6) is multiplied with a constant $e^{-j\theta}$. The θ refers to the synchronous rotating angular speed of the rotatory reference frame, ω_r. Thus, it result as (7).

$$\vec{v}_v^r = R_{f1} \vec{i}_v^r + L_{f1} \frac{d\vec{i}_v^r}{dt} + R_{f2} \vec{i}_g^r + L_{f2} \frac{d\vec{i}_g^r}{dt} + \vec{v}_g^r + j\omega_r L_{f1} \vec{i}_v^r + j\omega_r L_{f2} \vec{i}_g^r \tag{7}$$

The superscript r of (7) means for electrical quantities referring to rotatory reference frame. By decomposing (7) into dq components, the vector orientation of the VSI are formulated:

$$v_{dv} = R_{f1}i_{dv} + L_{f1}\frac{di_{dv}}{dt} + R_{f2}i_{dg} + L_{f2}\frac{di_{dg}}{dt} + v_{dg} - \omega_r L_{f1}i_{qv} - \omega_r L_{f2}i_{qg} \qquad (8)$$

$$v_{qv} = R_{f1}i_{qv} + L_{f1}\frac{di_{qv}}{dt} + R_{f2}i_{qg} + L_{f2}\frac{di_{qg}}{dt} + v_{qg} + \omega_r L_{f1}i_{dv} + \omega_r L_{f2}i_{dg} \qquad (9)$$

the dq- voltage vectors given in (8) and (9) are properly align with grid voltage space vector as:

$$v_{dg} = |\vec{v}_g| \qquad (10)$$

$$v_{qg} = 0 \qquad (11)$$

the synchronous rotating angular speed, ω_r, is set equal to the angular speed of the grid voltage, ω. Hence, (8) and (9) can be simplified as (12), (13).

$$v_{dv} = R_{f1}i_{dv} + L_{f1}\frac{di_{dv}}{dt} + R_{f2}i_{dg} + L_{f2}\frac{di_{dg}}{dt} + v_{dg} - \omega L_{f1}i_{qv} - \omega L_{f2}i_{qg} \qquad (12)$$

$$v_{qv} = R_{f1}i_{qv} + L_{f1}\frac{di_{qv}}{dt} + R_{f2}i_{qg} + L_{f2}\frac{di_{qg}}{dt} + \omega L_{f1}i_{dv} + \omega L_{f2}i_{dg} \qquad (13)$$

This paper adopts the decoupled current compensation and voltage feed-forward compensation techniques to simplify (12) and (13). In addition, the fundamental component of the converter-side current, i_{xv}, and grid-side current, i_{xg}, are assumed equivalent. Hence, the dynamic models of the recuperating system can be finalized as:

$$v_{dv} = R_{f1}i_{dg} + L_{f1}\frac{di_{dg}}{dt} + R_{f2}i_{dg} + L_{f2}\frac{di_{dg}}{dt} \qquad (14)$$

$$v_{qv} = R_{f1}i_{qg} + L_{f1}\frac{di_{qg}}{dt} + R_{f2}i_{qg} + L_{f2}\frac{di_{qg}}{dt} \qquad (15)$$

based on the developed dynamic model, a pair of PI-controller is introduced to regulate the grid current as shown in Figure 3, where Figures 3(a) and 3(b) present the respective current regulators in d-axis and q-axis. The PI-controller is employed with two main controlled objectives. The controller must ensure zero steady state error and offer good dynamic response. The open-loop and close-loop transfer functions.

$$G_{OL}(s) = \left(K_P + \frac{K_i}{s}\right) \cdot \left(\frac{1}{s(L_{f1}+L_{f2})+(R_{f1}+R_{f2})}\right) \qquad (16)$$

$$G_{CL}(s) = \frac{sK_P + K_i}{s^2(L_{f1}+L_{f2})+s(R_{f1}+R_{f2}+K_P)+K_i} \qquad (17)$$

The controller gain, K_p and K_i can be determined by equaling the denominators of (17) with the generalized transfer function of a second-order system. These gains can then be formulated as:

$$K_i = (L_{f1} + L_{f2})\omega_n^2 \qquad (18)$$

$$K_p = 2\zeta\omega_n(L_{f1} + L_{f2}) - (R_{f1} + R_{f2}) \qquad (19)$$

where ζ and ω_n represent the damping ratio and natural frequency of a second order system.
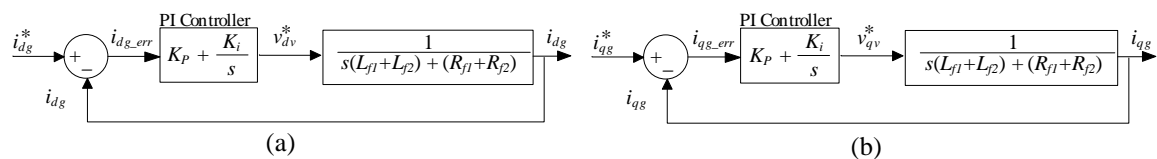

Figure 3. Current regulators with PI-controller (a) i_{dg} and (b) i_{qg}

3. CONTROLLER GAIN TUNNING AND ANALYSIS

The PI controller gains are tuned based on a set of LCL-filter parameters given in Table 1 [11]. This paper proposes to design the PI controller with two equal real poles ($\zeta=1$). The natural frequency, ω_n, is proposed to be set at one order of magnitude smaller than the VSI switching frequency. The K_i and K_p are calculated as 287.80 and 0.67. The PI controller is then analyzed in the frequency and time domains as shown in Figure 4. Figure 4(a) shows the Bode plots of (16) and (17) with the calculated gains. The cut-off frequency, f_c, is measured at 275 Hz. The phase margin is estimated as 77°. Since the phase margin is greater than 60°, a stable dynamic response is being expected. The close-loop bandwidth is assumed equal to the cut-off frequency of the open-loop transfer function. In summary, the close-loop bandwidth is fall under the permitted range of the LCL-filter design [11]. Figure 4(b) shows a step-response of the current regulator. When the input change is detected, the PI controller shows a fast transient response with 0.88 ms rise time is measured. An overshoot of 12.7% is detected at 2.37 ms. Finally, the controller reaches the settling time of 6.3 ms. The final value of the step-response is shown at the amplitude of one, which confirmed the objective of zero steady state error is met.

Table 1. System parameters

| Voltage source inverter		LCL-filter	
DC-link voltage, V_{dc}	900 V	Converter side inductor, L_{f1}	300 μH
DC-link capacitor, C_{dc}	1 mF	Converter side inductor internal resistance, R_{f1}	7.50 mΩ
PWM switching frequency, f_{sw}	1350 Hz	Grid side inductor, L_{f2}	100 μH
Amplitude modulation index, m_a	1.15	Grid side inductor internal resistance, R_{f2}	2.50 mΩ
Rated nominal AC voltage, v_{ab}	585 V	Filter capacitor, C_f	1.00 mF
Rated fundmental frequency, f_g	50 Hz	Damping resistor, R_d	0.05 Ω

(a)

(b)
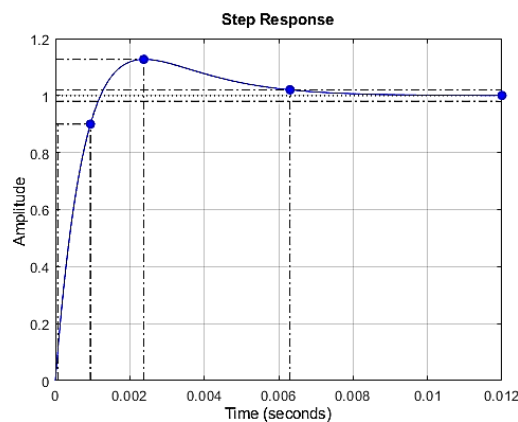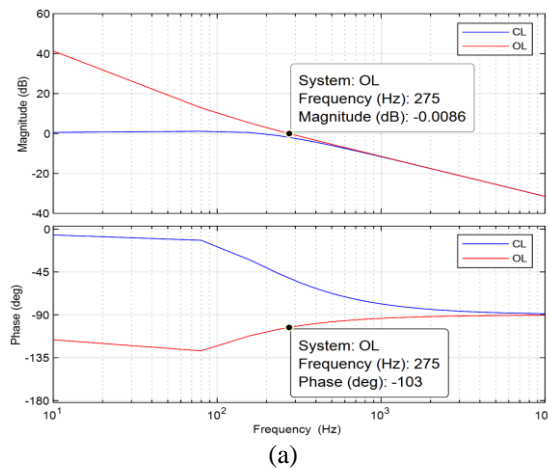
Figure 4. PI controller analysis (a) bode plots of open loop (OL) and close loop (CL) and (b) step response of the current controller

4.   SYSTEM LEVEL SIMULATION AND ANALYSIS

The proposed vector control strategy is evaluated via MATLAB/Simulink simulation software. Figure 5 shows the simulation model built for the proposed system. The DC power recuperating system is modelled as shown in Figure 5(a) with the VSI power circuit is presented in Figure 5(b). All the simulation parameters are configured as listed in Table 1. The GVOVC and THVI-PWM scheme are depicted in Figure 5(c). Three-phase balance grid voltages rated at 585 V, 50 Hz are used as the reference voltages for the GVOVC.
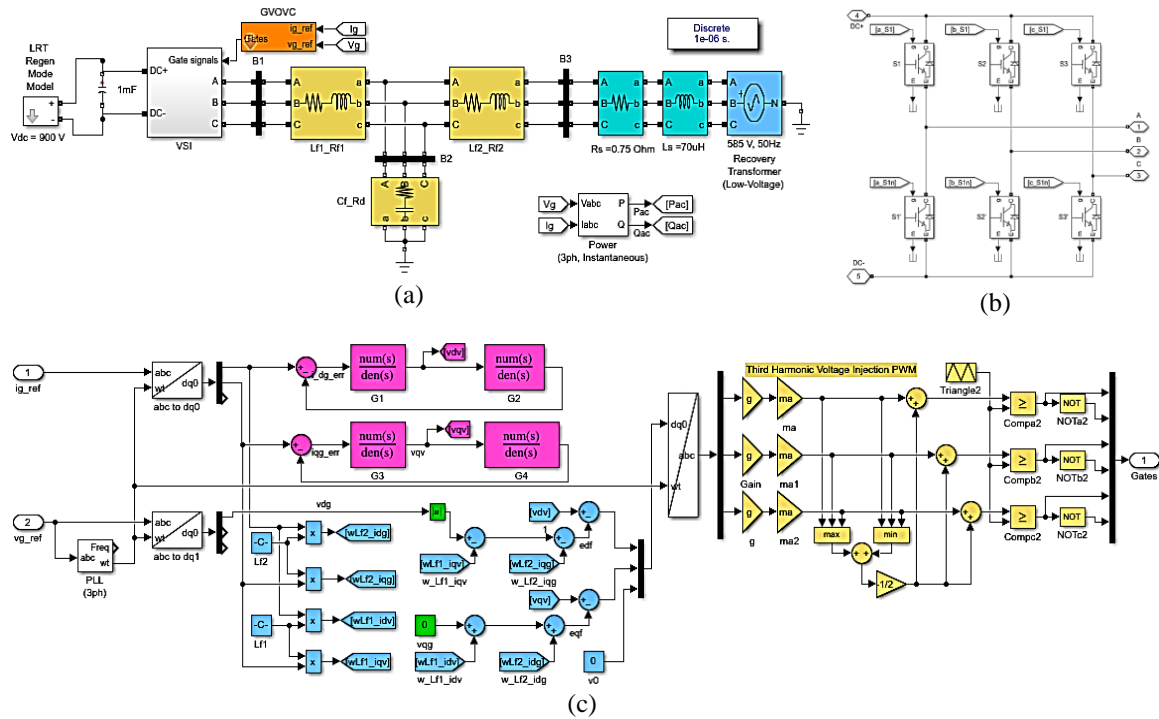

(a)

(b)

(c)

Figure 5. Simulation model of; (a) recuperating converter system, (b) VSI, and (c) GVOVC and THVI-PWM

The angular speed of the grid is extracted using the phase lock loop module. This angular speed is then used as input to *abc-dq* transformation blocks. The *dq*-currents controller blocks (magenta blocks) consist of the PI-controller (G1 and G3) and the dynamic model of the VSI (G2 and G4). The transfer function G1–G4 are identical to the block shown in Figure 3. The *dq*-voltages of the VSI (light-blue color blocks) can then be estimated using (15) and (16). The estimated *dq*-reference voltages are inversely transformed back to *abc*-domain before modulating. The estimated *abc*- reference voltages are first being normalized and then set to the desired amplitude modulation index, m_a. In this simulation, the m_a is fixed at the ratio of 1.15. The THVI-PWM model is developed based on the formulation given in [23]. The modulating waves are then compared with a 1350 Hz triangular carrier wave to generate a series of gate pulses for the VSI.

The simulation model is programmed to initially run with the conventional sinusoidal pulse width modulated inverter (SPWM) scheme [11]. The proposed GVOVC scheme is activated when the simulation time reaches 0.15s. Figure 6 shows the simulation results of three-phase voltage and current waveforms captured at buses *B1*, *B2*, and *B3* (Figure 5 (a)). As shown in Figure 6(a), the VSI produces badly distorted AC voltages and currents at bus *B1*. The distortion is mainly due to the switching frequency set in kilo Hertz range. By using the fast fourier transform (FFT) analyzer of the simulation software, both voltages and currents total harmonic distortion (THD) are measured at 68.75% and 7.25%. The designated LCL-filter had mitigated the switching distortion. Figure 6(b) presents the voltages and currents at bus *B2*, it is noted that the high switching ripple currents are being drained out by the filter capacitor effectively. As a result, good quality of grid voltages and currents are captured at bus *B3*, as shown in Figure 6(c). The GVOVC scheme is enable upon reaching the simulation time of 0.15 s. The VSI encountered light fluctuation from 0.15 s until 0.157 s. This has proven that the controller gains are tunned correctly to ensure the system reaching its steady state witin 7 ms. The amplitude of the grid voltages is amplified to about 490 V (peak) after entering steady state. This is mainly due to effect of THVI-PWM.
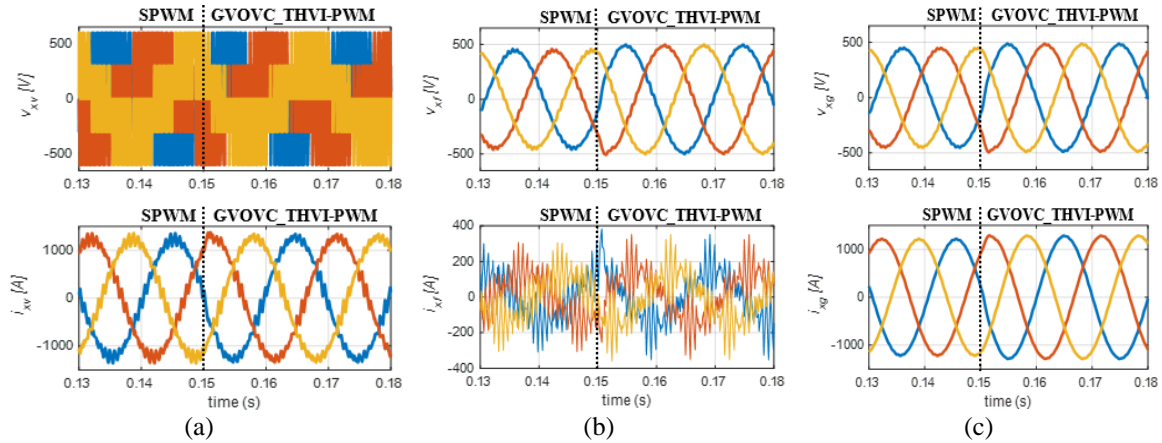
Figure 6. Simulation results of voltage and current waveforms measured at; (a) B1 (converter-side),
(b) B2 (filter capacitor in series with damping resistance), and (c) B3 (grid-side)

Figure 7 shows the harmanic spectrums for grid voltages and current at bus *B3*, before and after the activation of GVOVC with THVI-PWM. The voltage and current harmonic indexes are recorded less than 2%. With SPWM control scheme, the most significant harmonics components are captured around the frequency modulation index and its multiples as shown in Figure 7(a). Whereas, with the proposed control scheme, some lower order harmonics ($3<h<19$) are captured in Figure 7(b). This is mainly due to the effect of injecting the third harmonic voltage into the modulating wave. Fortunately, all individual harmonics components percentage are kept lower than the IEEE standard [25].
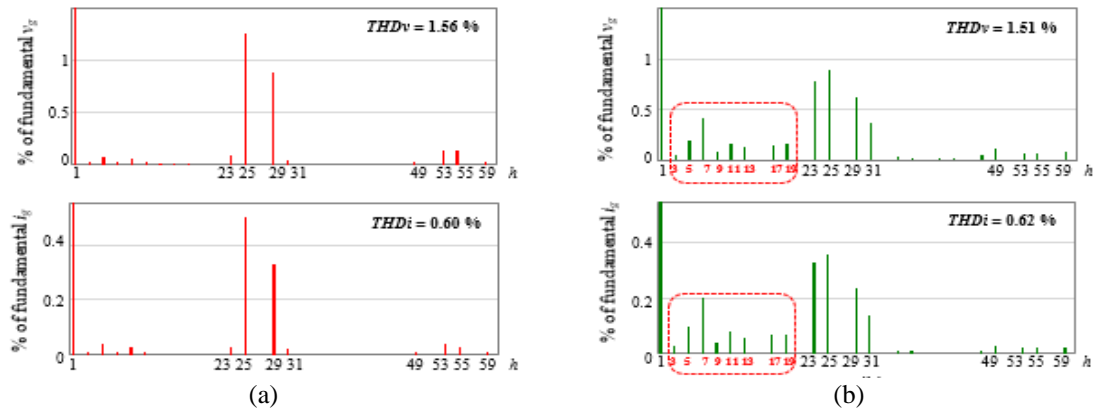

Figure 7. Harmonic spectrum of grid voltages captured at bus *B3* (Figure 8 (c)) (a) SPWM and
(b) GVOVC_THVI-PWM

Figure 8 shows the *dq*-axes of grid voltages and currents results which are used to further analyse the instantaneous active and reactive power variations at bus *B3*. Prior to 0.15 s, the recuperating converter is being controlled using SPWM method. As shown in Figure 8(a), the *dq*-componenets of the grid voltages yields an average of 420 V and 150 V. When GVOVC and THVI-PWM scheme are enable, v_{dg} is increased to an average of 482 V. This is mainly due to the effect of amplitude modulation index had been set to 1.15, which resulting of 14.76% of grid voltage (*d*-component) amplification. On the other hand, with the reference v_{qg} is fixed to 0 V, the *q*-component of grid voltage is captured closed to 0 V once the system operates in steady state mode. The *dq*-grid currents show similar changes as if the grid voltages, the respective waveforms are presented in Figure 8(b). Lastly, Figure 8(c) presents the instantaneous power delivered to the utility grid. The proposed control and modulation scheme manage to increase approximately 16% of the active power, P_{ac}, to the utility grid. Besides, the lagging power factor had been corrected after enabling the proposed control scheme. When the system is stable, the simulation result as shown in Figure 8(c) shows a leading power factor, which extends future works in the area of reactive power exchange with the utility grid [8].
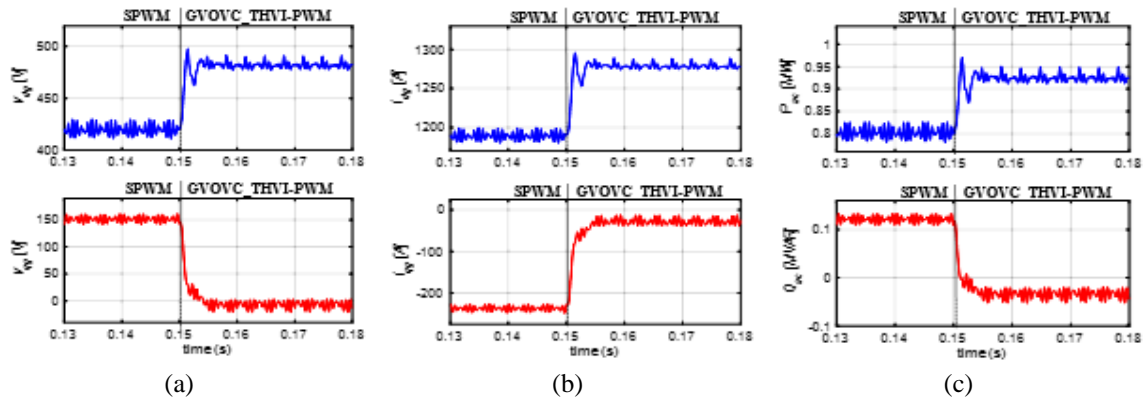
Figure 8. Instantaneous waveforms of; (a) *dq*-voltages, (b) *dq*-currents, and (c) active and reactive power

5. CONCLUSION

This paper presents a simulation study of a recuperating converter control scheme used in a DC traction power substation. With the objective to feed-in the regerative power harvested by a train to an energized grid, the GVOVC with THVI-PWM scheme had been proposed. The mathematical modeling and design of the controller had been presented. The feasibility of the proposed controller had been validated via simulation analysis. The simulation study shows that good quality of three-phase AC voltages and currents are produced at the point of common coupling. The voltage and current harmonics distortion indexes are recorded at 1.51% and 0.62%. The proposed THVI-PWM technique offers further adjustment of the AC voltage amplitude to not more than 15%. Since the proposed controller permits independent control of the voltage quantities in *dq* reference frame, the regulation of active and reactive powers could be realized.

REFERENCES

[1] S. A. Assefa, A. B. Kebede, and D. Legese, "Harmonic analysis of traction power supply system: case study of Addis Ababa light rail transit," *IET Electrical Systems in Transportation*, vol. 11, no. 4, pp. 391–404, May 2021, doi: 10.1049/els2.12019.

[2] S. Milovanovic, S. Strobl, P. Ladoux, and D. Dujic, "Hardware-in-the-loop modeling of an actively fed MVDC railway systems of the future," *IEEE Access*, vol. 9, pp. 151493–151506, 2021, doi: 10.1109/ACCESS.2021.3125050.

[3] S. Sharifi, T. Kamel, and P. Tricoli, "Investigating the best topology for traction power substations (TPSs) in a medium voltage DC (MVDC) railway electrification system," Sep. 2021, doi: 10.23919/epe21ecceeurope50061.2021.9570403.

[4] C. L. Toh and C. W. Tan, "DC traction power substation using eighteen-pulse rectifier transformer system," *International Journal of Power Electronics and Drive Systems*, vol. 12, no. 4, pp. 2284–2394, Dec. 2021, doi: 10.11591/ijpeds.v12.i4.pp2284-2294.

[5] M. Brenna, F. Foiadelli, and H. J. Kaleybar, "The evolution of railway power supply systems toward smart microgrids: the concept of the energy hub and integration of distributed energy resources," *IEEE Electrification Magazine*, vol. 8, no. 1, pp. 12–23, Mar. 2020, doi: 10.1109/MELE.2019.2962886.

[6] Z. H. Choi, Z. H. Toh, and M. H. B. Z. Hilmi, "Comparative study of two potential recuperating converters in dc railway electrification system for harmonic mitigation," *International Journal of Power Electronics and Drive Systems*, vol. 10, no. 3, pp. 1157–1166, Sep. 2019, doi: 10.11591/ijpeds.v10.i3.pp1157-1166.

[7] Z. Tian, G. Zhang, N. Zhao, S. Hillmansen, P. Tricoli, and C. Roberts, "Energy evaluation for DC railway systems with inverting substations," *In 2018 IEEE International Conference on Electrical Systems for Aircraft, Railway, Ship Propulsion and Road Vehicles & International Transportation Electrification Conference,* Nov. 2019, doi: 10.1109/ESARS-ITEC.2018.8607710.

[8] M. Popescu and A. Bitoleanu, "A review of the energy efficiency improvement in DC railway systems," *Energies*, vol. 12, no. 6, p. 1092, Mar. 2019, doi: 10.3390/en12061092.

[9] G. Zhang, Z. Tian, P. Tricoli, S. Hillmansen, Y. Wang, and Z. Liu, "Inverter operating characteristics optimization for DC traction power supply systems," *IEEE Transactions on Vehicular Technology*, vol. 68, no. 4, pp. 3400–3410, 2019, doi: 10.1109/TVT.2019.2899165.

[10] A. Jitpaiboon, T. Kulworawanichpong, and T. Ratniyomchai, "Energy saving of a DC railway system by applying inverting substations," in *2021 International Conference on Power, Energy and Innovations,* 2021, pp. 85–88, doi: 10.1109/ICPEI52436.2021.9690646.

[11] N. A. Sabran, C. L. Toh, and C. W. Tan, "LCL-filter design and analysis for PWM recuperating system used in DC traction power substation," *International Journal of Power Electronics and Drive Systems*, vol. 13, no. 4, pp. 2244–2254, 2022, doi: 10.11591/ijpeds.v13.i4.pp2244-2254.

[12] M. F. Yaakub, M. A. M. Radzi, M. Azri, and F. H. M. Noh, "LCL filter design for grid-connected single-phase flyback microinverter: A step by step guide," *International Journal of Power Electronics and Drive Systems*, vol. 12, no. 3, pp. 1632–1643, Sep. 2021, doi: 10.11591/ijpeds.v12.i3.pp1632-1643.

[13] M. Popescu, A. Bitoleanu, and A. Preda, "A new design method of an LCL filter applied in active DC-traction substations," *IEEE Transactions on Industry Applications*, vol. 54, no. 4, pp. 3497–3507, Jul. 2018, doi: 10.1109/TIA.2018.2819968.

[14] S. Harasis *et al.*, "Enhanced dynamic performance of grid feeding distributed generation under variable grid inductance," *International Journal of Electrical and Computer Engineering*, vol. 12, no. 2, pp. 1113–1122, Apr. 2022, doi: 10.11591/ijece.v12i2.pp1113-1122.

[15] M. H. Z. Hilmi, C. L. Toh, and P. C. Ooi, "Modelling and design of a current controller for light rail regenerative inverter system," in *CENCON 2019 - 2019 IEEE Conference on Energy Conversion*, 2019, pp. 18–23, doi: 10.1109/CENCON47160.2019.8974714.

[16] S. Aatif, H. Hu, X. Yang, Y. Ge, Z. He, and S. Gao, "Adaptive droop control for better current-sharing in VSC-based MVDC railway electrification system," *Journal of Modern Power Systems and Clean Energy*, vol. 7, no. 4, pp. 962–974, Jan. 2019, doi: 10.1007/s40565-018-0487-0.

[17] V. H. Avila and V. Leite, "Control of grid-connected inverter output current: a practical review," in *9th International Conference on Renewable Energy Research and Applications,* Sep. 2020, pp. 232–235, doi: 10.1109/ICRERA49962.2020.9242710.

[18] M. T. Faiz, M. M. Khan, J. Huawei, M. A. Mumtaz, M. U. Shahid, and T. Houjun, "H∞ robust control with improved harmonics suppression for inverter-based distributed generation systems," *IET Power Electronics*, vol. 13, no. 13, pp. 2742–2755, Sep. 2020, doi: 10.1049/iet-pel.2019.1408.

[19] Q. Liu, T. Caldognetto, and S. Buso, "Review and comparison of grid-tied inverter controllers in microgrids," *IEEE Transactions on Power Electronics*, vol. 35, no. 7, pp. 7624–7639, Jul. 2020, doi: 10.1109/TPEL.2019.2957975.

[20] X. Yang, H. Hu, Y. Ge, S. Aatif, Z. He, and S. Gao, "An improved droop control strategy for VSC-based MVDC traction power supply system," *IEEE Transactions on Industry Applications*, vol. 54, no. 5, pp. 5173–5186, Sep. 2018, doi: 10.1109/TIA.2018.2821105.

[21] G. Guo *et al.*, "Application of third-order harmonic voltage injection in a modular multilevel converter," *IEEE Transactions on Industrial Electronics*, vol. 65, no. 7, pp. 5260–5271, Jul. 2018, doi: 10.1109/TIE.2017.2777413.

[22] S. S. K. Kenny, R. T. Naayagi, S. S. Lee, and C. Shuyu, "Three phase VSI control system rapid prototyping with TI C2000 MCU and PLECS coder," *5th International Conference on Green Energy and Applications,* 2021, pp. 42–46, doi: 10.1109/ICGEA51694.2021.9487561.

[23] C. L. Toh and P. C. Ooi, "Design a nine-level modular multilevel converter for DC railway electrification system," *International Journal of Power Electronics and Drive Systems*, vol. 11, no. 1, pp. 151–159, Mar. 2020, doi: 10.11591/ijpeds.v11.i1.pp151-159.

[24] A. Milicua and G. Abad, "Control of grid-connected converters," *Power Electronics and Electric Drives for Traction Applications*. Wiley, pp. 148–220, Sep. 2016, doi: 10.1002/9781118954454.ch4.

[25] "IEEE recommended practice and requirements for harmonic control in electric power systems," in *IEEE Std. 519-2014 (Revision of IEEE Std 519-1992)*, pp. 1–29, June 2014, doi: 10.1109/ieeestd.2014.6826459.

BIOGRAPHIES OF AUTHORS

Chuen Ling Toh received the B. Eng. and M. Eng. degree in electrical engineering, both from Universiti Teknologi Malaysia (UTM), Skudai, Malaysia, in 2002 and 2005 respectively; and her Ph.D. in Electrical Power Engineering from Norwegian University of Science and Technology (NTNU), Trondheim, Norway, in 2014. Currently, she is a Senior Lecturer at the Universiti Tenaga Nasional, Kajang, Malaysia. Her teaching and research interests include the field of power electronics, motor drive systems and field programmable gate array applications. She is also an engineer registered with Board of Engineers Malaysia and a professional technologist registered with Malaysia Board of Technologists. She can be contacted at email: chuenling@uniten.edu.my.

Chee Wei Tan received his B.Eng. degree in Electrical Engineering (First Class Honors) from Universiti Teknologi Malaysia (UTM), in 2003 and a Ph.D. degree in Electrical Engineering from Imperial College London, London, U.K., in 2008. He is currently an associate professor at Universiti Teknologi Malaysia and a member of the Power Electronics and Drives Research Group, School of Electrical Engineering, Faculty of Engineering. His research interests include the application of power electronics in renewable/alternative energy systems, control of power electronics and energy management system in microgrids. He is also a Chartered Engineer registered with Engineering Council, UK, a professional engineer registered with Board of Engineers Malaysia and a professional technologist registered with Malaysia Board of Technologists. He is actively participating in IEEE activities and conferences, which he is also the chair of the IEEE Power Electronic Society (PELS) Malaysia Chapter for year 2018. He was awarded the Malaysia Research Star Award (High Impact Paper–Engineering and Technologies) 2018 by the Ministry of Education Malaysia. He can be contacted at email: cheewei@utm.my.